

Article

Online Feet Potential Fields for Quadruped Robots Navigation in Harsh Terrains

Viviana Morlando , Jonathan Cacace  and Fabio Ruggiero 

Department of Electrical Engineering and Information Technology, University of Naples Federico II,
Via Claudio 21, 80125 Naples, Italy; jonathan.cacace@unina.it (J.C.); fabio.ruggiero@unina.it (F.R.)

* Correspondence: viviana.morlando@unina.it

Abstract: Quadruped robots have garnered significant attention in recent years due to their ability to navigate through challenging terrains. Among the various environments, agriculture fields are particularly difficult for legged robots, given the variability of soil types and conditions. To address this issue, this study proposes a novel navigation strategy that utilizes ground reaction forces to calculate online artificial potential fields, which are then applied to the robot's feet to avoid low-traversability regions. The strategy also incorporates the net vector of the attractive potential field towards the goal and the repulsive field to avoid slippery regions, which dynamically adjusts the quadruped's gait. A realistic simulation environment validates the proposed navigation framework with case studies on randomly generated terrains. A comprehensive comparison with baseline navigation methods is conducted to assess the effectiveness of the proposed approach.

Keywords: motion control; potential fields; quadruped navigation



Citation: Morlando, V.; Cacace, J.; Ruggiero, F. Online Feet Potential Fields for Quadruped Robots Navigation in Harsh Terrains. *Robotics* **2023**, *12*, 86. <https://doi.org/10.3390/robotics12030086>

Academic Editor: Chengxu Zhou

Received: 29 April 2023

Revised: 8 June 2023

Accepted: 11 June 2023

Published: 13 June 2023



Copyright: © 2023 by the authors. Licensee MDPI, Basel, Switzerland. This article is an open access article distributed under the terms and conditions of the Creative Commons Attribution (CC BY) license (<https://creativecommons.org/licenses/by/4.0/>).

1. Introduction

With the ability to adjust their footstep and overcome obstacles, legged robots are well-suited to tasks that must be performed in challenging terrains, such as industrial plant inspection, search and rescue, precision agriculture [1], and similar. Recently, research has emphasized the development of agile gaits, enhancing the capacity to maintain steadiness during motion to replicate living beings' natural movement. Although there have been considerable advancements in motion planning and control techniques, legged robots are still incapable of dealing with all the challenges posed by unstructured environments and unknown terrains. For this reason, it becomes essential for them to ensure stability and adjust their foothold as per the unevenness and ruggedness of the ground.

While much progress has been made navigating non-flat terrains [2,3], ensuring stable and effective walking in rough and slippery areas is still challenging for legged systems. As an additional complexity, terrain features that characterize the roughness and density of the walking surface are difficult to identify by exploiting vision-based information that can be misleading or not detailed enough. The main aim of this work is to make an online estimate of the so-called traversability of the terrain that the legged system is trampling, calculating the best direction to overcome low-traversability regions and, at the same time, reach a target position. The traversability index can generally be considered a metric describing the robot's ease of navigating a terrain. It can refer to the ability of a robot to navigate through a particular environment or surface. This includes the ability to overcome obstacles and challenges such as slopes, stairs, uneven surfaces, and other impediments. Path planner algorithms can use terrain traversability metrics to ensure effective navigation. Nevertheless, the estimation of this metric relies on exteroceptive sensors such as LIDARs, depth cameras, cameras, and so on. Because of this, it does not provide information about the collapsibility of the terrain, but only a semantic classification of its type, while field robots must be able to navigate over pitfalls covered with leaves, plants on soft soil and water puddles.

In this work, we propose an approach in which a quadruped robot can perform a traversability analysis during navigation, similar to how living beings push their feet into the ground to evaluate if they can safely walk over a given region. To replicate the natural behaviour of living beings, an online potential field is computed at each footstep. In this way, the robot tries to reach a given (pre-planned) goal (attractive potential) while, at the same time, it tries to avoid low-traversability regions (repulsive potential). The combination of the attractive and repulsive forces, adequately tuned, drives the legged robot during the navigation. Each foot's stability is evaluated during the stance phase to provide information about the terrain. The stability is measured by considering the distance of the vertical component of the ground reaction forces from the friction cone boundaries. This acts as a robustness index, indicating the likelihood of feet sliding and causing an imbalance. The integral of each foot's robustness index during the stance phase, also known as the average robustness, is used to compute a repulsive potential field. This field pushes the robot away from the position of less stable feet and towards more stable ones. In addition, the resultant repulsive potential field is used to switch the gait type. Indeed, different gaits can be performed during quadruped locomotion, realising more or less dynamic movements. Usually, if the robot moves only one leg at a time, the performed gait is called crawl. This is an intrinsically stable form of walking, since three legs are always standing. Instead, highly dynamic movements can be performed whenever two legs are moving contemporarily: trot gait, when diagonal pairs of legs move together; pace gait, with lateral pairs of legs moving contemporarily; and gallop gait, when either the front legs or the rear ones swing simultaneously. In this paper, the nominal performed gait will be the trot, since it is the one that best conjugates a more stable movement with the capability to reach highly dynamic and fast locomotion. However, there could be the chance that, in complex situations, all the feet fall in a low-stability condition, and the repulsive field is insufficient to find a direction that brings the robot far from the low-traversability region. In this case, when the robustness index of the four feet starts to decrease under a certain threshold, the gait is switched to a more stable one (i.e., the crawl one) to traverse this region while increasing the overall stability.

To summarise, the provided contributions against state-of-the-art approaches are (i) an estimation of the traversability of the terrain trampled by the robot during the navigation. This estimation is performed for each foot of the quadruped robot to analyse the terrain comprehensively; (ii) implementation of a navigation function based on the traversability analysis to adapt the executed path online to reach a given target traversing a safe path.

To assess the effectiveness of the proposed approach, a set of simulation test cases have been carried out in the Gazebo dynamic simulator, considering environments populated with regions with different slipperiness. In all the tests, a pre-defined goal point has been selected and the capacity to avoid low-traversability regions has been determined, along with an estimation of the stability of the legged system during the locomotion.

The remainder of the paper is organised as follows. Section 2 presents a brief overview of the state of the art of similar applications. In Section 3, the dynamic model of a quadruped robot is presented, while in Section 4, the deployed system architecture is detailed along with a discussion of the proposed approach from a theoretical and practical point of view. Finally, in Section 5, a set of case studies is discussed to demonstrate the effectiveness of the proposed approach.

2. Related Works

Quadruped robots have become increasingly prevalent in various fields, ranging from laboratory research [4–6] to practical industrial applications [7]. Despite their diverse applications, legged robots face the common challenge of maintaining stability during locomotion on unstructured, rugged, and complex terrains. A typical control approach to enable the navigation of quadruped robots is to consider the control in the operational space. This is a popular method that considers the entire dynamics of a robot. This

method entails imposing desired motion for pertinent points such as the centre of mass or reference points for the feet [2,8,9]. Improving the performance of low-level controllers and ensuring stable robot locomotion can be achieved by finding the best path and footholds during navigation. In this field, various techniques have been proposed. For instance, in [10], an online force-based foothold adaptation mechanism is presented to update the planned motion based on the perceived state of the environment. In [11], a heightmap is created and utilised by a D^* planner algorithm to generate path regions that are easy to navigate. Such regions are known as high-traversability regions and represent those parts of the terrain that can be easily traversed. Traversability analysis (See [12]) typically uses vision, LIDARs, or depth sensors. This process calculates the ability of a terrain to be traversed; it has been studied in different research works and emerged as a widely adopted method with which to evaluate diverse environments. It comprehensively evaluates various terrain features such as slope and roughness and combines them into a single metric [11,13]. Depending on the environmental features to identify, different approaches can be employed. In [14], the authors proposed a LIDAR-based approach for semantic terrain classification. Based on this classification, a probabilistic traversability map is generated. Similarly, in [13], a hierarchical traversability analysis where point cloud-based step segmentation and geometric slope–roughness metrics are unified into one cost map, while semantic information, geometry information, and robot mobility are fused in [15] to provide an estimation of the traversability. Moreover, identifying outdoor terrains with only visual information, such as soft soil or deep water, remains challenging. For this reason, in our work, the robot can estimate the traversability of the region of terrain that is trampled by using the ground reaction forces.

The authors in [15] utilised a quadruped robot equipped with a probing arm to evaluate the traversability metric of the terrain. They executed this by using the force sensor integrated at the end of the probing arm to push on the terrain. The methodology applied in their work resembles our approach of verifying the terrain consistency using contact. However, our approach distinguishes itself from theirs because it does not need a probing arm and computes the traversability at every step.

In this work, information about the traversability of the terrain is used in a navigation function implemented in the artificial potential field (APF). APF in robotics finds its foundation in [16]. Since then, this technique has been extensively leveraged to resolve the path planning problem for various industrial manipulators and mobile robots [17–19]. With its intuitive physical implications and modelling, coupled with its simplicity, robustness, and real-time performance, the APF approach has become a well-researched and highly utilized tool in robotics. Potential fields continue to offer the most suitable solution for mobile robot navigation in cluttered environments. In this navigation context, the robot's target point acts as an attractive force, while obstacles around the robot act as repulsive forces [20]. Researchers have explored different approaches to making this field model more effective so that the robot can exhibit a range of behaviours during navigation. For instance, in [21], a combined potential field model with five components (like target, land, back, car, and speed potentials) is proposed. Additionally, in [22,23], researchers have developed an application for aerial and industrial robots that enables human operators to change the robot's trajectory while maintaining attractive forces towards a destination point and a pre-planned path. The repulsive force in the proposed approach is directly generated by the traversability of the terrain, which dynamically changes during navigation. In this way, executing the most efficient path becomes easier, paving the way for optimal navigation [13,24].

3. Dynamic Model

3.1. Model Formulation

A legged robot can be assimilated to a free-floating base with some limbs attached to it. The base can be modelled using six virtual joints, providing the system with six unactuated degrees of freedom (DoFs) with respect to a fixed world frame \mathcal{W} (see Figure 1). These

DoFs represent the pose of the robot base, while each leg provides the system with other $n > 0$ joints. Then, if $n_l \geq 2$ legs are attached to the floating base, the robot has a total of $nn_l + 6$ DoFs.

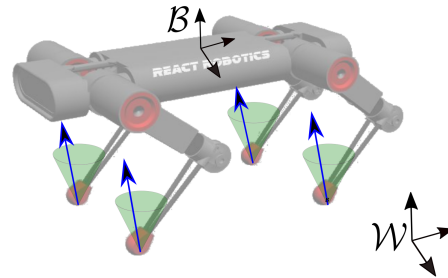


Figure 1. DogBot, the platform used for simulations. The reference frames for the robot are shown. Ground reaction forces (in blue) need to stay in the cones (in green).

Either a point fixed on the base or the centre of mass (CoM) of the robot can be considered to represent the position of the system [25]. In the following explanation, the centroidal dynamics of a legged robot will be presented, considering the position of the system coinciding with the position of the CoM. With this purpose, let \mathcal{B} be the frame whose position is attached to the robot’s CoM (see Figure 1), with $x_{com} = [x_c \ y_c \ z_c]^T \in \mathbb{R}^3$, $\dot{x}_{com} \in \mathbb{R}^3$, and $\ddot{x}_{com} \in \mathbb{R}^3$ the position, velocity, and acceleration of the CoM with respect to \mathcal{W} , respectively. The orientation of the frame \mathcal{B} can be considered the one of a fixed frame on the main body, expressed with respect to \mathcal{W} by the rotation matrix $R_b \in SO(3)$, from which the set of ZYX Euler angles $\phi \in \mathbb{R}^3$ can be extracted. Moreover, let $\omega_{com} \in \mathbb{R}^3$ and $\dot{\omega}_{com} \in \mathbb{R}^3$ be the angular velocity and the angular acceleration of \mathcal{B} with respect to \mathcal{W} , respectively. Finally, indicate with $q \in \mathbb{R}^{nn_l}$ the vector collecting the legs’ joints.

Considering the assumptions that the main body’s angular motion is slow and that the legs’ mass is negligible with respect to the robot’s total mass, the centroidal dynamic model of a legged robot assumes a decoupled structure, as introduced in [26]. The inertia matrix assumes the structure $M(q) = \begin{bmatrix} M_{com}(q) & O_{6 \times nn_l} \\ O_{nn_l \times 6} & M_q(q) \end{bmatrix} \in \mathbb{R}^{6+nn_l \times 6+nn_l}$. In this way, the decoupling of the centroidal term $M_{com}(q) \in \mathbb{R}^{6 \times 6}$ is clearly distinguished from the one related to the legs $M_q(q) \in \mathbb{R}^{nn_l \times nn_l}$. As a consequence of the previously introduced assumptions, the Coriolis and centrifugal terms related to the angular part of the CoM can be neglected [2,25]. Thus, the vector accounting for Coriolis, centrifugal and gravitational forces is $h(q, v) = \begin{bmatrix} O_{6 \times (6+nn_l)} \\ C_q(q, v) \end{bmatrix} v + \begin{bmatrix} mg \\ 0_{nn_l} \end{bmatrix}$, with $C_q(q, v) \in \mathbb{R}^{nn_l \times (6+nn_l)}$, where $v = [\dot{x}_{com}^T \ \omega_{com}^T \ \dot{q}^T]^T \in \mathbb{R}^{6+nn_l}$ is the stacked velocity; $m > 0$ is the total mass of the robot, $g = [g_0^T \ 0_3^T]^T \in \mathbb{R}^6$, and $g_0 \in \mathbb{R}^3$ the gravity vector; 0_{\times} and O_{\times} the zero vector and matrix of proper dimensions, respectively. The resultant model can be written as

$$M(q)\dot{v} + h(q, v) = S^T \tau + J_{st}(q)^T f_{gr}, \tag{1}$$

with $S = [O_{nn_l \times 6} \ I_{nn_l}] \in \mathbb{R}^{nn_l \times (6+nn_l)}$ a selection matrix; $\tau \in \mathbb{R}^{nn_l}$ the joint actuation torques; $f_{gr} \in \mathbb{R}^{3n_{st}}$ are the ground reaction forces, with $0 < n_{st} \leq n_l$ the number of stance legs; $J_{st}(q) = [J_{st,com}(q) \ J_{st,j}(q)] \in \mathbb{R}^{3n_{st} \times 6+nn_l}$ where $J_{st,com}(q) \in \mathbb{R}^{3n_{st} \times 6}$ and $J_{st,j}(q) \in \mathbb{R}^{3n_{st} \times nn_l}$ are those Jacobians whose transpositions map the ground reaction forces into the acceleration of the CoM and the legs’ joints, respectively. Further details about the above matrices’ expressions can be found in [25,27,28]. It can be noticed that the dynamics of the CoM are decoupled from the ones of the legs, so that the CoM’s dynamics, also called centroidal dynamics, are included in the first six rows of Equation (1).

3.2. Friction Cone

When analysing the design of a legged robot, it is crucial to prioritise the interaction between the machine and the ground to achieve effective locomotion and balance. The contact with the terrain provides valuable feedback regarding the robot’s current stability and balance, which is particularly significant when executing complicated gaits requiring high dynamism.

The interaction is primarily influenced by the friction coefficient between the ground and the robot’s feet. This is because the Coulomb’s friction model dictates that each of the robot’s feet has two distinct behaviours during the stance phase of contact [29], namely:

- Fixed contact if the ground reaction force $f_{gr,i}$ is contained within the boundaries of the relative friction cone;
- Sliding contact if the ground reaction force $f_{gr,i}$ is not contained within the boundaries of the relative friction cone.

Each foot in contact with the ground generates a friction cone that starts from the point of contact, as illustrated in Figure 1. The size of the friction cone depends on the friction coefficient μ . Specifically, let \vec{n}_i denote the unit normal to the ground at the i -th contact point. The friction cone associated with this foot is aligned along \vec{n}_i . Additionally, let $\vec{t}_{i,1}$ and $\vec{t}_{i,2}$ represent two tangential vectors at the i -th contact point. The friction cone manifold can be defined as follows [30]

$$FC_i = \left\{ f_{gr,i} \in \mathbb{R}^3 : \sqrt{(f_{gr,i}\vec{t}_{i,1})^2 + (f_{gr,i}\vec{t}_{i,2})^2} \leq \mu f_{gr,i}\vec{n}_i, \quad f_{gr,i}\vec{n}_i \geq 0 \right\}, \quad (2)$$

where the boundary of the manifold δFC_i represents the boundary of the friction cone. If $f_{gr,i}$ falls outside this boundary, the foot starts sliding. Having this in mind, it becomes apparent that the friction coefficient μ plays a crucial role in determining the stability of the robot. A higher coefficient enlarges the friction cone manifold, reducing the likelihood of sliding.

However, if the robot does start to slide on the ground, the system’s balance can no longer be considered stable. If the feet begin to lose traction, there is a significant chance that the quadruped will struggle to maintain balance, eventually leading to a fall. To accurately measure the robot’s ability to resist sliding and determine its overall robustness during movement, consideration can be given to the distance of the ground reaction forces from the boundary of the friction cone manifold δFC_i . This can be achieved by calculating the angle between the normal i -th contact and the corresponding contact force using $\alpha_i = \arccos(\vec{n}_i^T f_{gr,i} / \|f_{gr,i}\|)$. The semi-aperture angle of the i -th friction cone, denoted as $\theta_i = \arctan \mu$, is also considered. By combining these factors, the boundary of the i -th friction cone manifold can be expressed as [6,31]

$$\delta FC_i = \left\{ f_{gr,i} \in \mathbb{R}^3 : |\alpha_i| = \theta_i \right\}. \quad (3)$$

It can be deduced that the distance between the i -th ground reaction force vector and the cone boundary can be expressed as the distance of α_i from θ_i . Based on these findings, a metric used to assess the robustness of the i -th foot at the instant t during the locomotion can be formulated as

$$\mathcal{R}_i(t) = \theta_i - |\alpha_i(t)|. \quad (4)$$

In this study, the robustness index will be utilised as a part of an APF to determine the repulsive force, which will steer the robot away from areas with low friction coefficients where slipping may occur. The aim is to guide the robot towards regions with a higher friction coefficient and robustness index for enhanced stability and effectiveness.

4. System Architecture

The proposed control framework has been implemented using the system architecture presented in Figure 2. Herein, the legged robot is simulated using Gazebo simulator software (version 11.1), a realistic physical simulator in robotics. The virtual platform comprises a 12-DoF robot with four legs, where effort motor controllers are emulated. The whole-body controller module [2,32] computes the 12 torque values, τ , to control the platform. The simulator output comprises various data, such as the estimation of the centre of mass position, p_{com} , its velocity, \dot{p}_{com} , and the position and velocity of the robot joints, $q \in \mathbb{R}^{12}$ and $\dot{q} \in \mathbb{R}^{12}$, respectively. The whole-body controller module leverages these data to calculate the control input at each time step, and this module comprises a motion planner and an optimization problem.

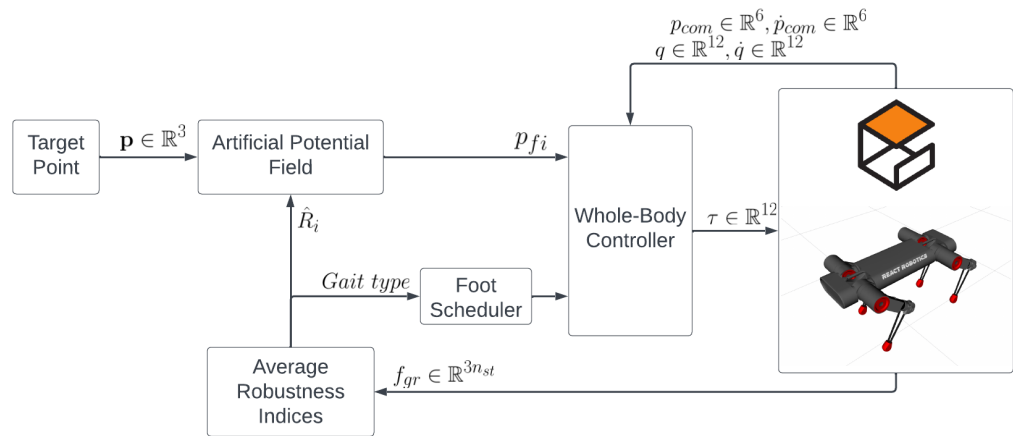


Figure 2. The scheme is representing the system architecture.

Figure 2 illustrates that the foot scheduler determines the order and timing of each foot’s movement. In the context of quadruped robot locomotion, a step can be defined as having two phases: the stance phase, when all feet are in contact with the ground; and the swing phase, when some feet are moving [2,32]. During each step, the foot scheduler schedules the timing of these phases. After the conclusion of each step, the motion planner within the whole-body controller calculates trajectories for both the feet and the CoM of the robot for the next step. To accomplish this, the motion planner uses the scheduling generated by the foot scheduler and the desired foot positions for the next step, which the APF module determines.

The platform boasts four force sensors for each foot which generate a ground reaction force when in contact with the ground during the stance phase, denoted by $f_{gr} \in \mathbb{R}^{3nst}$. The Average Robustness Indices module employs these data to compute each foot’s average robustness indices ($r_{1,...,4}$). Additionally, the module calculates the metrics for all four feet, enabling the selection of a desired gait type based on a tuned threshold for average robustness indices. Specifically, if the mean among all foot indices is lower than the given threshold, the system will choose a safer gait type. In this study, the robot alternates between trot and crawl. This last, being a more precautionary gait type, ensures that the robot maintains its stability on slippery surfaces.

The APF module uses the average robustness indices along with a target point, $p_{com,des} \in \mathbb{R}^3$, to generate the attractive and repulsive potential fields. Based on the resultant field, the desired position of each foot at the end of the next step is calculated (p_{f_i} , with $i = 1, \dots, 4$). The whole-body controller module uses the feet position to calculate the new position of the body, pushing the robot toward the force field. Indeed, the desired position of the feet is passed to the whole-body controller, together with the system output from the simulator. Starting from these data, the motion planner within the whole-body controller computes a trajectory for both the feet and the CoM for the next step. Therefore, this trajectory is used as input for the optimization problem to compute the robot’s

commands while respecting constraints related to dynamic consistency, mechanical safety, and non-slippage conditions. For detailed information about the whole-body controller module, see [2,32].

4.1. Feet Potential Field

The potential field approach is frequently employed in robot motion planning to achieve a specific goal while also adhering to safety directives, e.g., avoiding obstacles or navigating hazardous areas. To create a trajectory for the robot to follow, the potential function is determined by adding up two potentials:

- The attractive potential: a potential field that pushes the robot towards the goal;
- The repulsive potential: a repulsive field that pushes the robot away from obstacles or other dangerous regions.

This approach is commonly used in mobile robotics to enable the robot to continuously plan its motion in real time while relying on partial information about its environment. Typically, a mobile robot position is represented by a single fixed point on its base, and this point is moved as per the computed potential field. However, only considering a fixed control point attached to the robot base fails to serve the purpose of this research, which aims to devise a navigation algorithm that accounts for the robot's balance stability during motion. To accomplish this objective, it is crucial to consider a potential field around each robot's foot. As outlined in Section 3.2, one of the most critical aspects in achieving balance stability in a legged robot relates to the friction cone of each contact point. Therefore, the previously defined robustness index can be a helpful indicator of the traversability of the region currently being traversed by the robot. Based on the value of this index for each foot, a safer direction of movement can be computed to steer away from the most slippery terrain, drawing inspiration from the natural behaviour of animals. These animals rely on sensing the softness or sliding of the terrain while pushing their feet and use this information to determine their next steps [33,34]. This approach is a novel way to ensure stability in the navigation of the robot. Hence, the approach adopted in this study involves the computation of a potential field for each robot's foot. This field is designed to impart directional forces that enhance the stability of individual legs on the ground. This, in turn, improves the robot's overall ability to maintain balance effectively.

When dealing with a quadruped robot and its stance phase stability, a crucial factor to consider is establishing a sound and reliable nominal stable configuration. This configuration can be seen as the robot's ultimate goal, which it should strive to achieve once the desired position has been attained. In essence, it is the key to ensuring optimal stability throughout the robot's operations. Let us consider the position of the CoM on the x - y plane (see Figure 3), denoted as $p_{xy,com} = [x_c \ y_c]^T \in \mathbb{R}^2$. In a nominal configuration, the positions of the four feet on the same plane can be expressed as $p_{f,i}^* = p_{xy,com} + \delta p_{f,i} \in \mathbb{R}^2$, where i denotes the corresponding foot. To achieve a stable configuration, the desired position for each foot can be computed as $p_{f,i,des} = x_{com,des} + \delta p_{f,i} \in \mathbb{R}^2$ when the robot reaches its desired goal at $x_{com,des}$. The potential field for each foot is composed of two terms, namely:

- The attractive potential bringing the i -th foot towards the goal $p_{f,i,des}$;
- The repulsive field that exploits the robustness index of the foot.

The attractive force can be computed considering a paraboloidic potential [35]. Consider the error from the desired position of the i -th foot as

$$e_{f,i} = p_{f,i} - p_{f,i,des}. \quad (5)$$

Then the attractive force of the foot can be computed as

$$f_{a,i} = k_a e_{f,i}, \quad (6)$$

where $k_a \in \mathbb{R}$ is an attractive gain.

To accurately calculate the repulsive field for each foot, it is crucial to determine the appropriate direction in which the field must be directed. To achieve this, it is necessary to push the entire robot structure away from areas with a higher degree of slipperiness. The four-unit vectors depicted in Figure 3, which extend from each foot to the CoM, must therefore be considered. The i -th unit vector can be written as

$$\vec{d}_{com,fi} = \frac{p_{f,i} - p_{xy,com}}{\|p_{f,i} - p_{xy,com}\|}. \tag{7}$$

These unit vectors represent the direction the individual foot must move to be pushed away from its current position, if necessary. Let us consider the robustness index of the i -th foot at instant t , denoted as $\mathcal{R}_i(t)$. The repulsive force acting on this foot can be expressed as:

$$f_{r,i}(t) = \frac{1}{\mathcal{R}_i(t)} \vec{d}_{com,fi}, \tag{8}$$

meaning that the force applied must be inversely proportional to the index. For instance, if the foot is robust, it ought to be repulsed less while, if the foot is less robust, it should be pushed more from its current position.

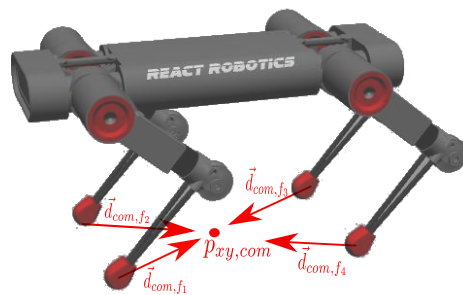


Figure 3. Repulsive unit vectors for the four feet of the quadruped.

A sequential movement of the robot trajectory is illustrated in Figure 4. Upon inspection, it is evident that the final direction of the robot is primarily determined by the resultant force acting on the CoM of the repulsive and attractive fields. In a scenario where the robustness of all feet is the same (i.e., the friction coefficient is identical), the repulsive force acting on the CoM is nullified, and the robot only follows the attractive potential, heading towards the goal. However, if one foot is less robust than the others, the resultant force will impact the entire structure, leading it towards the direction of the repulsive fields while still tracking the attractive potential.

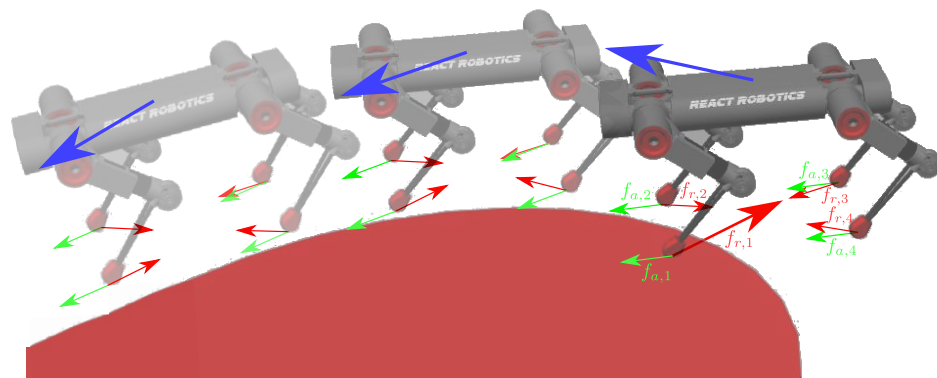


Figure 4. Sequential movement of the robot trajectory to avoid a low traversability region, using the proposed approach. In red, the repulsive forces; in green, the attractive ones. Blue arrows indicate the resultant direction of the robot.

Consider the scenario depicted in Figure 4. At the start, the front left foot encounters a surface with a lower friction coefficient than the other feet, leading to a decrease in stability and an increase in the magnitude of its repulsive force. Consequently, the robot follows the direction indicated by the blue arrow, pushing the robot away from the slippery region and towards safer and more traversable areas. It is worth noting that as the robot continues its trajectory, the repulsive fields of all four feet become equal, allowing it to track the attractive field.

The potential field calculation takes place at the conclusion of each step phase, just before the next motion planning stage. Consequently, the robustness computed at this point can be viewed as an average value for the period between two successive steps. Assuming a fixed step duration of Δt , at instant t , the average robustness over the interval from the beginning of the current step to t can be determined through the following expression:

$$\bar{\mathcal{R}}_i(t) = \Delta t^{-1} \int_{t-\Delta t}^t \mathcal{R}_i(\sigma) d\sigma. \tag{9}$$

This refers to the average robustness of the step phase. In other words, it is the robustness of the foot at the point where it is pushing. During the next trajectory planning, the repulsive field will guide the robot away from any slippery zones in its current stance. However, it is essential to note that if the average robustness only accounts for the current foot position, the trajectory planning may not consider the slipperiness of the previous foot positions. This increases the risk of the robot returning to a slippery region from which it had just navigated away due to an attractive potential. Hence, it is imperative to take into account the previous robustness values, which serve as an indicator of the slipperiness of the surrounding terrain. To mitigate this concern, an exponentially weighted moving average approach has been adopted [36,37]. This methodology relies on a procedure that mainly considers the most recent measurements, while older observations gradually lose their significance with time. The principle behind this approach is to compute a weighted average of all the past observations and use it to calculate the current average value $\hat{\mathcal{R}}_i(t)$. The mathematical expression for this estimation is presented below [36]

$$\hat{\mathcal{R}}_i(t) = \beta \left(\bar{\mathcal{R}}_i(t) + \gamma \bar{\mathcal{R}}_i(t - \Delta t) + \gamma^2 \bar{\mathcal{R}}_i(t - 2\Delta t) + \gamma^3 \bar{\mathcal{R}}_i(t - 3\Delta t) + \gamma^4 \bar{\mathcal{R}}_i(t - 4\Delta t) + \dots \right), \tag{10}$$

where $0 < \beta < 1$ and $\gamma = 1 - \beta$. By using this approach, we can ensure that the furthest points do not impact the current repulsive field. On the other hand, the closest points significantly impact the current robustness index, with the weight assigned based on the time of the footstep. The older the instant at which the footsteps are positioned, the less influence it has on the current robustness, thereby enhancing the stability of the robot. In order to simplify the computations, we can modify Equation (10) as follows [36]

$$\hat{\mathcal{R}}_i(t) = \beta \bar{\mathcal{R}}_i(t) + (1 - \beta) \hat{\mathcal{R}}_i(t - \Delta t). \tag{11}$$

In order to use Equation (11), the repulsive force in Equation (8) can be modified as

$$f_{r,i}(t) = \frac{1}{\hat{\mathcal{R}}_i(t)} \vec{d}_{com,f_i}. \tag{12}$$

The total potential force acting on the i -th foot is the sum of the attractive and repulsive ones

$$f_{p,i} = f_{a,i} + f_{r,i}. \tag{13}$$

From the potential force obtained for the next step, having assumed a fixed step duration of Δt , the i -th foot position can be computed as

$$p_{f,i} = p_{f,i} + \Delta t f_{p,i}. \tag{14}$$

4.2. Exit From Local Minima

In some situations, the robot could be trapped into local minima without being able to achieve the goal [35,38]. The proposed potential field approach may lead to an unforeseen situation if only two feet belonging to the same side of the robot (i.e., front, rear, left or right side) are standing on a slippery surface. In this case, the robot will be pushed in the opposite direction exiting from the slippery zone, but then the attractive potential field will push it again into the dangerous zone. Two indices can determine when the robot is in such a situation. These indices are derived from the combination of robustness indices computed for the feet. These include $\hat{\mathcal{R}}_{f1}$ for the front right foot, $\hat{\mathcal{R}}_{f2}$ for the front left foot, $\hat{\mathcal{R}}_{f3}$ for the rear right foot, and $\hat{\mathcal{R}}_{f4}$ for the rear left foot. The combined indices can be expressed as

$$\hat{\mathcal{R}}_{comb1} = |\hat{\mathcal{R}}_{f1} - \hat{\mathcal{R}}_{f2}| + |\hat{\mathcal{R}}_{f3} - \hat{\mathcal{R}}_{f4}|, \quad (15)$$

which represents the difference between the indices of the two front feet added to the difference between the indices of the two rear feet. The second considered index is

$$\hat{\mathcal{R}}_{comb2} = |\hat{\mathcal{R}}_{f1} - \hat{\mathcal{R}}_{f3}| + |\hat{\mathcal{R}}_{f2} - \hat{\mathcal{R}}_{f4}|, \quad (16)$$

representing the difference between the indices of the two right feet added to the difference between the indices of the two left feet. Consider a small value ϵ that represents the maximum difference in foot indices required for them to be considered in the same slipperiness region. Three situations can be identified, namely:

- $\hat{\mathcal{R}}_{comb1} < 2\epsilon$ and $\hat{\mathcal{R}}_{comb2} < 2\epsilon$, then all the feet are situated within a single slipperiness region;
- $\hat{\mathcal{R}}_{comb1} > 2\epsilon$ and $\hat{\mathcal{R}}_{comb2} < 2\epsilon$, then the left legs of the robot will be in an area with different levels of slipperiness compared to the right legs. This can result in the robot being stuck in a local minimum. If the right legs are in a more slippery region, the robot will be pushed to the left and then back to the right, remaining trapped in this repetitive movement. The applied strategy to overcome this situation is to move the feet either forward or backward (randomly chosen) until they are in the same region;
- $\hat{\mathcal{R}}_{comb1} < 2\epsilon$ and $\hat{\mathcal{R}}_{comb2} > 2\epsilon$. This indicates that the front legs of the robot are situated in an area with a different level of slipperiness compared to the rear legs. In such a scenario, the robot becomes stuck in a local minimum. When the front legs are placed in a slipperier region, the robot tends to move backwards before moving forward again, creating a cycle. To overcome this situation, the employed exit strategy is to move the robot towards the right or left side (randomly chosen) until all its feet are in the same region. Afterwards, the robot can move forward without being trapped.

5. Case Study

To evaluate the efficacy of the proposed methodology, simulations were conducted using Gazebo dynamic simulator and ROS noetic as the robotic programming framework [39]. The high-performance physics engine employed by Gazebo enabled the simulation of realistic robot movements and external conditions. This study utilised the DogBot model from React Robotics (see Figure 1), an open-source platform, as the quadruped for the simulations. Ground reaction forces were determined by integrating force sensors into the robot's feet. All simulations were performed on a standard PC running Ubuntu Linux 20.04. Four case studies were conducted, comprising two distinct types of testing. The first three cases were conducted to determine the effectiveness of the repulsive field as the robot traversed areas with differing friction coefficients, while the fourth case studied the dynamic gait change.

For each case study, a proper simulation scene has been set up. The robot must traverse zones with varying friction coefficients throughout the navigation process. The normal floor is assigned a friction coefficient of $\mu = 1$. Conversely, three different areas have been included, with friction coefficients μ of 0.8, 0.5, and 0.2, respectively. Each area has been marked with different colours in the simulation scenes for easy identification. Notably, the navigation challenge increases with a decrease in the coefficient index, meaning that areas with smaller coefficient indices pose more significant navigation difficulties for the robot. Since the actual μ coefficient of the area traversed during the navigation is unknown by the robotic system, a nominal $\mu = 0.5$ has been considered for the computation of the robustness index. The source code and the simulation environments used to perform the following simulations are accessible at this link: https://github.com/prisma-lab/APF_quadrupe (accessed on 12 June 2023).

5.1. Case Study 1

The effectiveness of the repulsive field in enhancing the average robustness index of each foot was evaluated in this case study. As shown in Figure 5, a simulation scene was configured with the robot's objective: traversing a straight path and reaching its target point. The robot initiated the test from the position $[0 \ 0]^T$ and aimed to reach the goal at $[0 \ -12]^T$. Three areas with different friction coefficients were placed along the path to simulate the slippery regions. These areas included a green area with $\mu = 0.8$, a blue area with $\mu = 0.5$, and a red area with a $\mu = 0.2$, all within 1 m radius circles. The test was then conducted twice, with and without activating the repulsive field. Results related to the test case are reported in Figure 6 when the repulsive field is enabled and Figure 7 when it is not. The monitored variables were the distance between the robot's body and the three areas, the average robustness for each foot, and the distance to the target. Comparing the two figures, using repulsive forces can increase the overall average robustness index, the meaningful parameter demonstrating the robot's stability. It could be observed that although the repulsive field causes the robot to deviate from the original path to remain in a region with a higher traversability, the overall duration of the trajectory is not highly affected. Figures 6a and 7a show that employing the repulsive field guarantees the robot will consistently remain within the circle's boundaries. This behaviour arises due to the potential field's ability to deflect the trajectory whenever the robot's feet make contact with the slippery surface. Consequently, the robot traverses a more stable region while maintaining proximity to the shorter path. To assess the improvements of our method over classical potential fields, we repeated the test 20 times with and without the repulsive field and monitored the mean value of the average robustness indices of all the feet. The mean values and standard deviation are reported in Table 1.

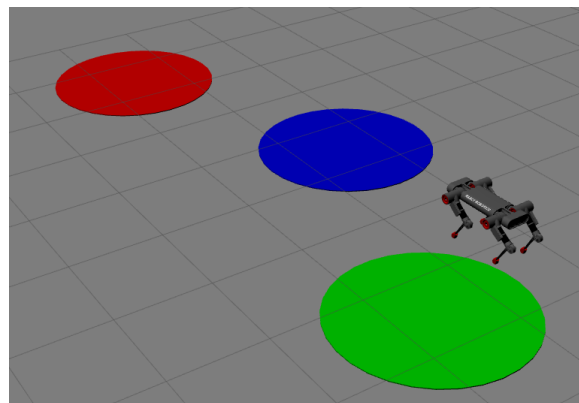
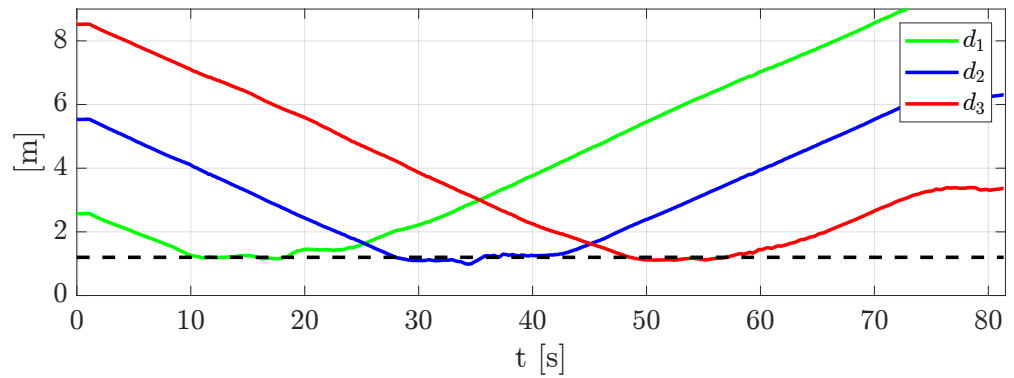


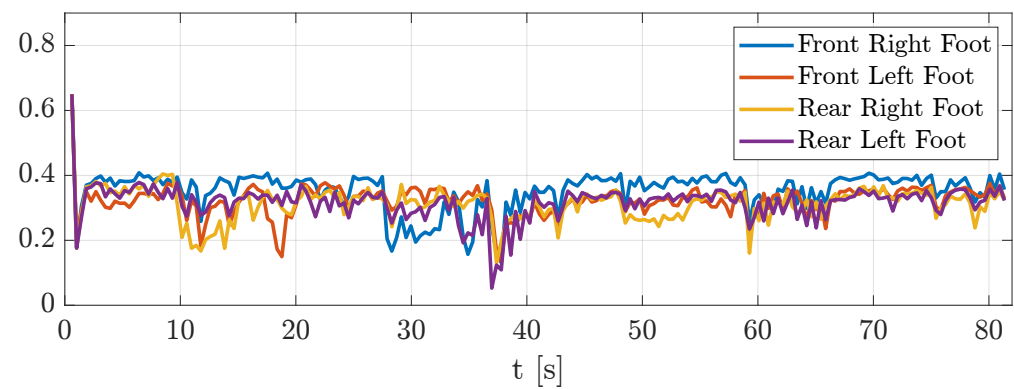
Figure 5. Case study 1. Three circle areas are included in the scene with the following friction coefficients: 0.8 for the green circle, 0.5 for the blue circle, and 0.2 for the red circle. The ground floor has 1.0 as the friction coefficient. A video showing the different case studies can be seen at this link: https://youtu.be/iUhhvo_zKuU (accessed on 12 June 2023).

Table 1. Mean value and standard deviation for the average robustness index with and without the repulsive field.

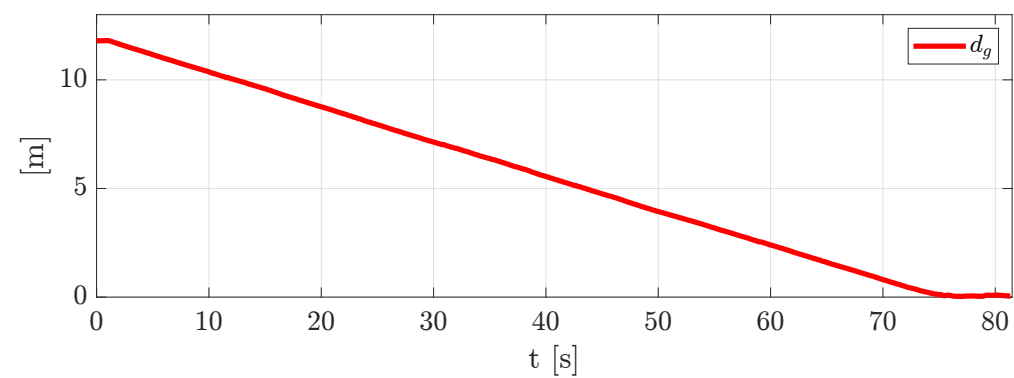
Test Mode	Average Robustness Index	Standard Deviation
Repulsive field ON	0.49	0.05
Repulsive field OFF	0.2	0.03



(a)



(b)



(c)

Figure 6. Results obtained for Case Study 1 enabling the repulsive field: (a) Distances from the centre of the three low-traversability areas; (b) robustness indices; (c) distance from the goal.

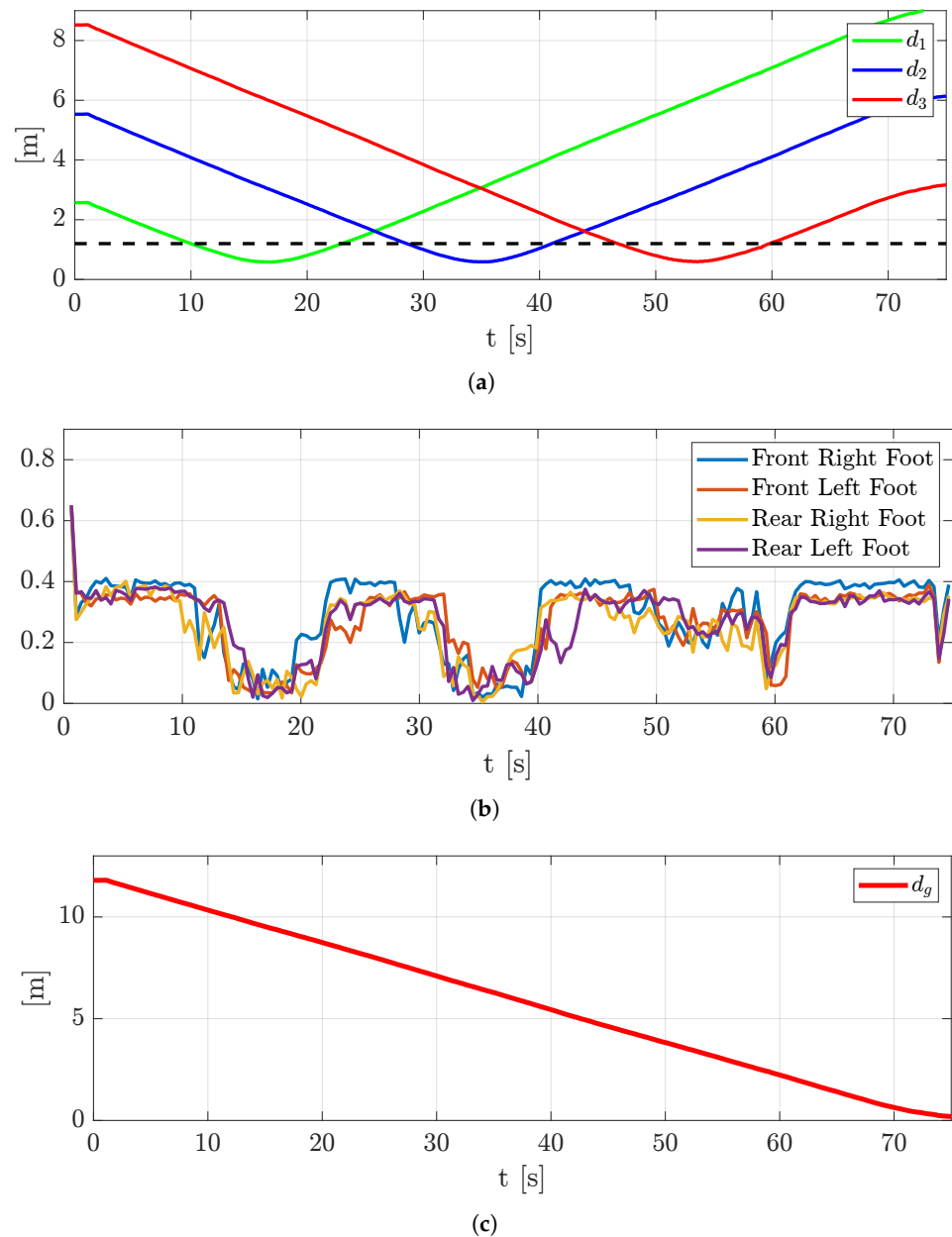


Figure 7. Results obtained for Case Study 1 without the repulsive field: (a) Distances from the centre of the three low-traversability areas; (b) Robustness indices; (c) Distance from the goal.

5.2. Case Study 2

The objective of the second case study is to evaluate the proposed control framework by selecting the area with the highest traversability, even when traversing slippery surfaces. Unlike the first case study, the quadruped is confined to walking in an area with a lower friction coefficient than the floor. The simulation environment is illustrated in Figure 8a, which includes three slippery surfaces. The robot’s goal is $[2 \ -9]^T$, whereas its starting position is the origin. Therefore, a diagonal linear path is necessary to reach the destination, forcing the robot to move to the right red area. The results from this test case are presented in Figure 9. The distance between the quadruped body and the two red areas is depicted in Figure 9a. In the beginning, the robot is repelled from the right red region (the red dashed line in Figure 9a), and it remains on the blue surface, maintaining a constant distance from the left red area until the quadruped overcomes it (vertical black dashed line in Figure 9a). This behaviour is also evident in the robustness indices in Figure 9a. It is essential to note

that deactivating the repulsive field for the same test is not feasible, as the quadruped platform topples due to the terrain’s high slipperiness.

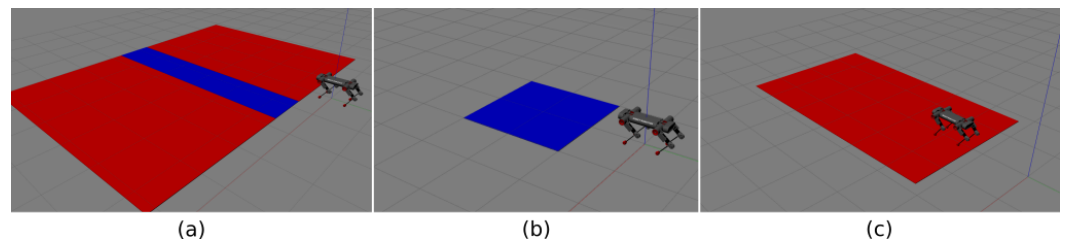


Figure 8. Simulated environments: (a) Case study 2; (b) Case study 3; (c) Case study 4. Two areas are included in the scenes with the following friction coefficients: 0.5 for the blue region, and 0.2 for the red one. The ground floor has 1.0 as the friction coefficient.

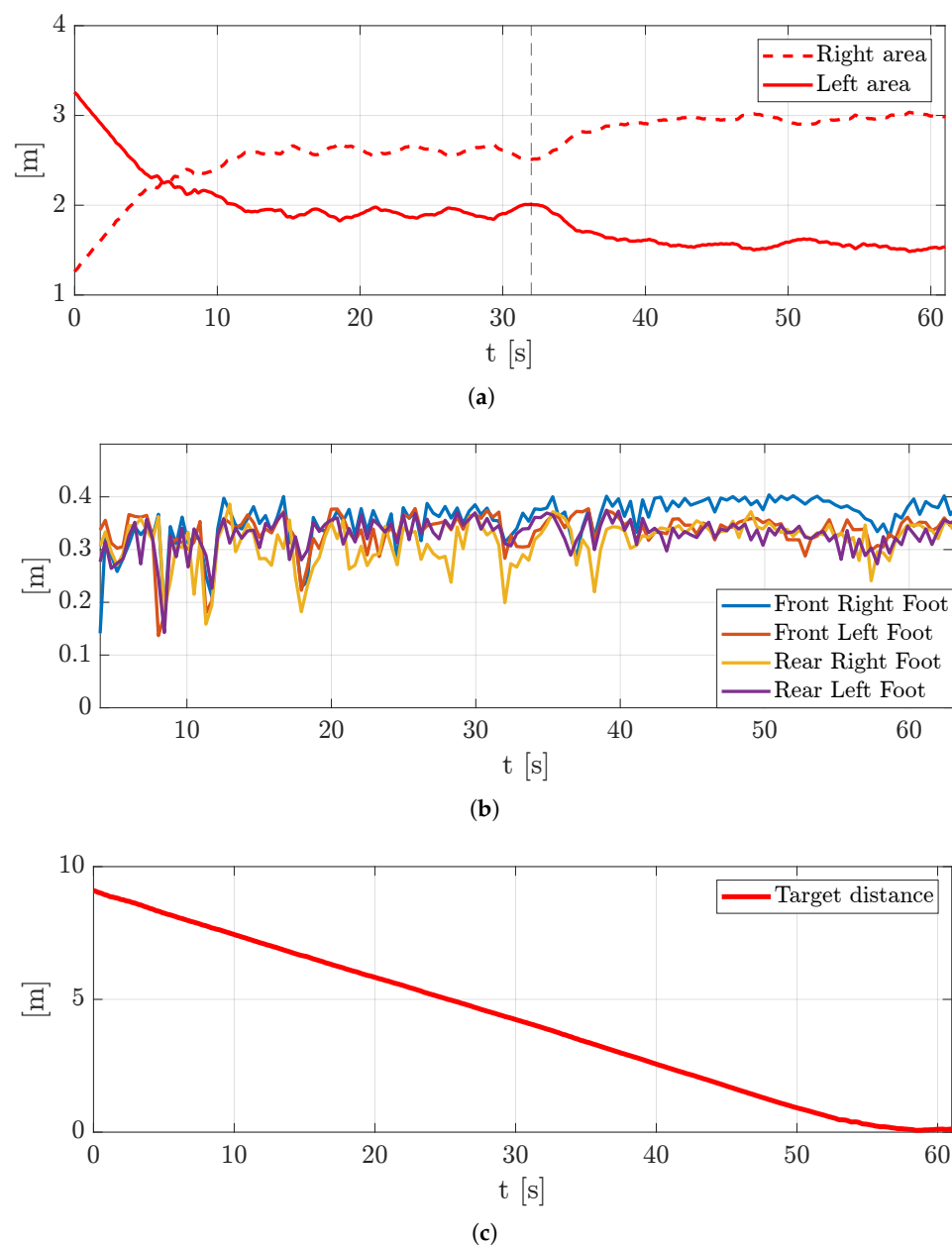


Figure 9. Results obtained for Case Study 2: (a) Distances from two low-traversability areas; (b) robustness indices; (c) distance from the goal.

5.3. Case Study 3

The goal of Case study 3 is to test the robot’s behaviour in the presence of local minima. The related simulation scene is reported in Figure 8b. As already stated (see Section 4.2), in the proposed approach, a local minima problem can occur when the two feet towards the direction of the attractive source trample at the same time a low-traversability area. This situation could create a neverending loop that causes the robot to get stuck. Then, this case study presents one of the cases of local minima considered, and the results are reported in Figures 10 and 11. In detail, setting the goal at $[0 \ -12]^T$ and looking at the scene in Figure 8b, it can be supposed that the robot will move forward, and at a certain point, both front feet will be placed on the slippery region. Therefore, the repulsive forces will push the robot back and forth in the blue region, trapping the robot. This behaviour is demonstrated by the plots in Figure 11, in which the system has been tested deactivating the local minima exit strategy. In particular, Figure 11a reports the distances from the goal and the centre of the blue area. It can be noticed that these distances remain constant during the test. The robot can overcome this difficulty once the exit strategy is applied. This can be seen in Figure 10, where the distances from the goal and the blue region and the robustness indices are reported. Initially, the distance from the centre of the blue area remains constant for a while, and the indices start to be lower than in the case of the standard floor ($\mu = 1$). This indicates that the exit strategy is being applied, and the robot is being pushed towards a random side direction while walking around the perimeter of the blue area. Finally, it can be affirmed that the robot exits from the local minimum condition when the distances from the goal and the centre of the slippery region start decreasing and increasing, respectively (vertical black dashed line in Figure 10a). In the meantime, the robustness indices increase.

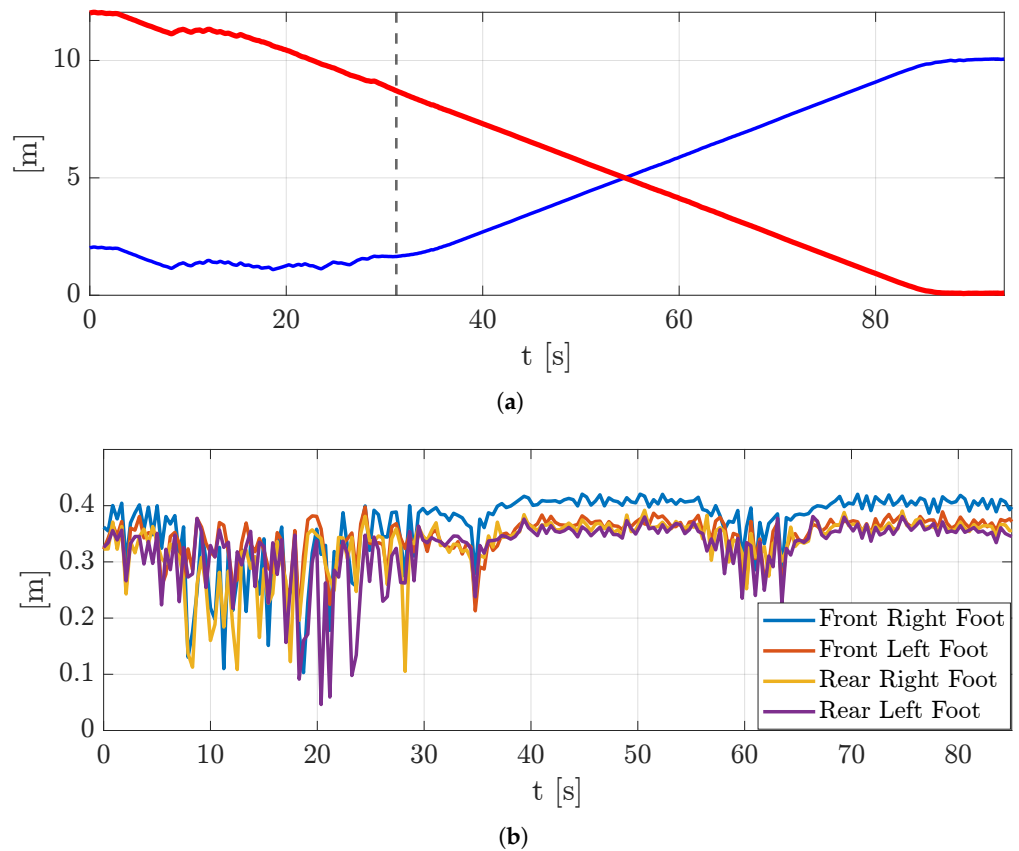


Figure 10. Results obtained for Case Study 3 applying exit strategy from local minima: (a) Distance from the target (red) and centre point of low-traversability area (blue); (b) robustness indices.

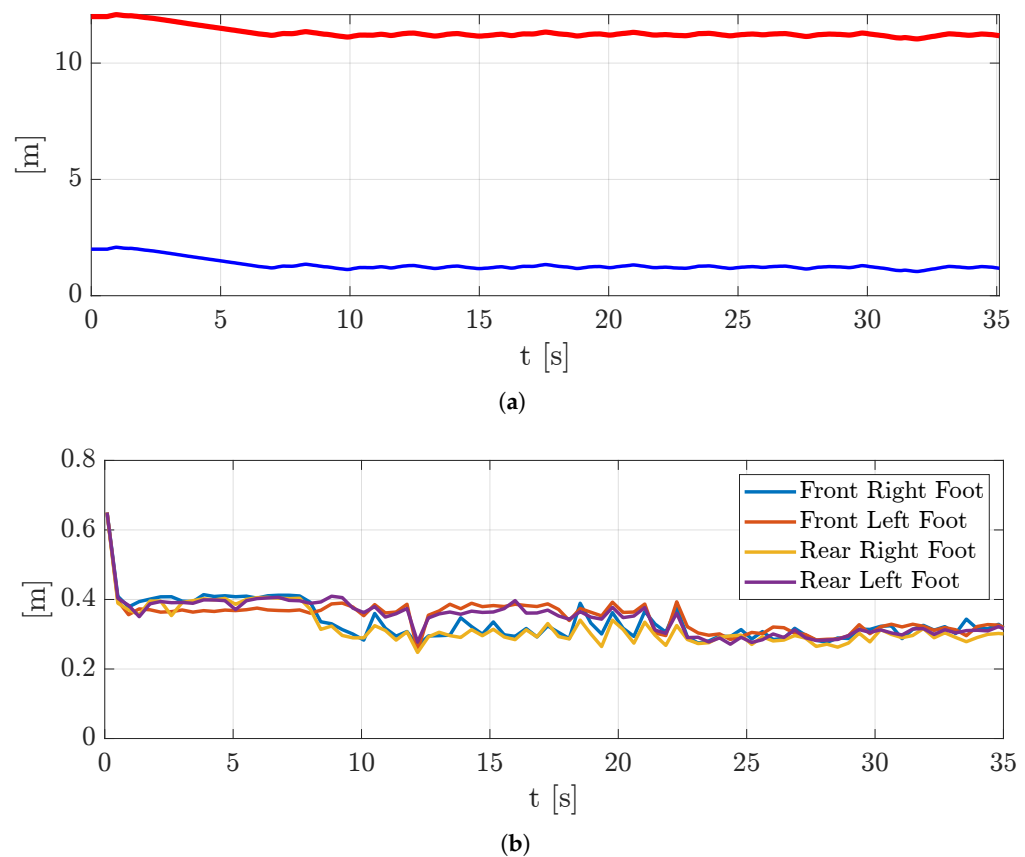
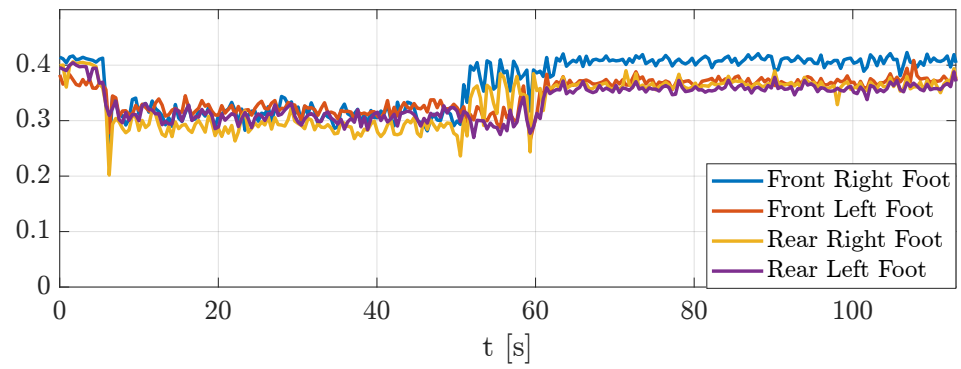


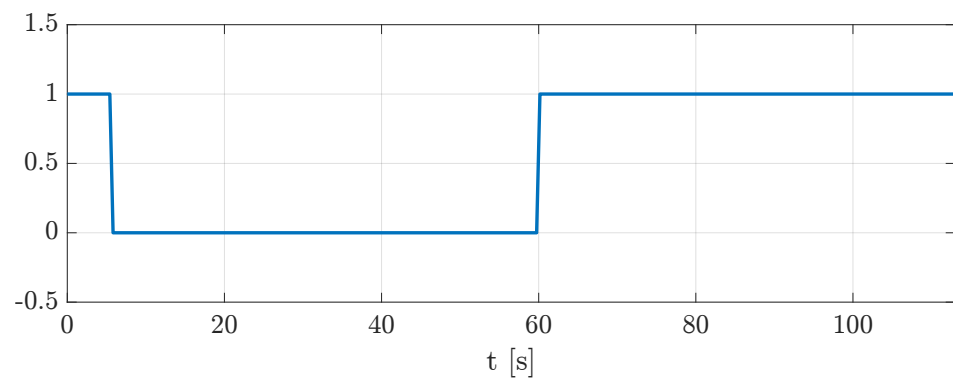
Figure 11. Results obtained for Case Study 3 without applying exit strategy from local minima: (a) Distance from the target (red) and centre point of low-traversability area (blue); (b) robustness indices.

5.4. Case Study 4

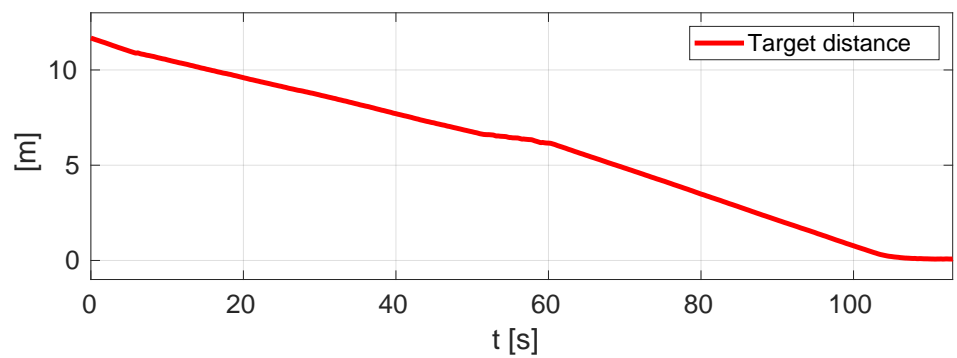
Case study 4 has been set up to test the gait change during the motion when the robot is trampling a low-traversability area with all its feet. The motivation behind this study is that whenever the exit strategy from local minima cannot bring the robot outside from the low-traversability region in a specific finite time, the robot should be forced to traverse this region to reach the goal. This means that the robot will find itself with all four feet on a slippery region. In this case, the indices of all the feet will decrease contemporarily under a certain threshold, and the robot is commanded to switch to a different gait type, such as the crawl (intrinsically stable), allowing the robot to traverse the whole region safely. Figure 8c reports the related simulation scene. The goal is $[0 \quad -12]^T$. In Figure 12, the results are reported. The robustness indices of the four feet can be seen in Figure 12a, while in Figure 12b, a flag representing the commanded type of gait is plotted. The flag is 1 when the trot command is implemented and 0 when it is switched to the crawl. It can be noticed that the gait switches when the robustness indices are all under a certain threshold that, in this work, is set as $\bar{r} = 0.35$. It should also be specified that a crawling gait is usually associated with a slower velocity, which guarantees more balance. This can be seen in Figure 12d, where the robot's velocity is reported. Indeed, when the gait flag is 0, the velocity is lower; it starts increasing again when it switches to trot and decreasing again only when it approaches the final goal. This is also confirmed by Figure 12c, representing the distance from the target.



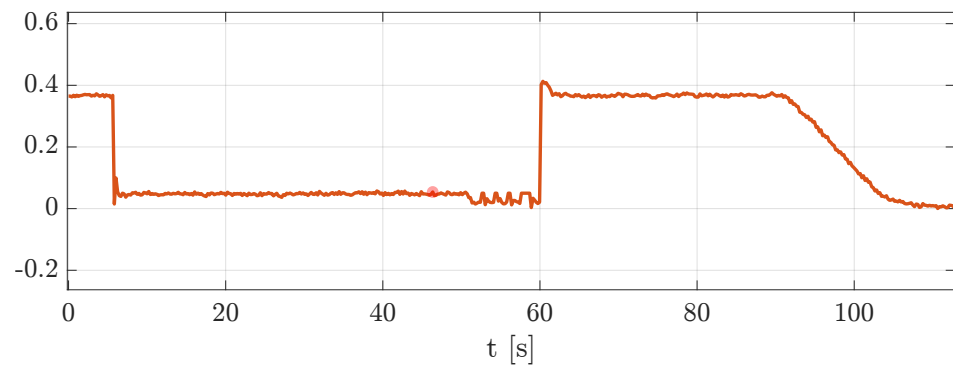
(a)



(b)



(c)



(d)

Figure 12. Results obtained for Case Study 4: (a) Robustness indices; (b) gait flag, 1 is for trot, 0 is for crawl; (c) distance from the target; (d) velocity of the robot.

6. Conclusions and Future Work

This work presents a novel approach to using artificial potential field techniques to drive the motion of a legged robot (i.e., a quadruped robot). The main novelty is calculating a repulsive force field based on the information of the ground reaction forces received from the quadruped during the navigation. These forces are adequately associated with an attractive force field to accomplish navigation tasks. The generated repulsive field allows for avoidance, when possible, of the navigation over low-traversability areas, preventing the robot from slipping on the ground and, consequently, achieving safer navigation. Starting from the ground reaction forces, the average robustness indices are used to calculate the repulsive forces for each foot of the robot. Finally, when the robot is constrained to walk over a low-traversability region, the mean of the average robustness indices is used to modulate the gait type, switching from a classic trot gait type to a more conservative one (i.e., the crawl). The proposed approach has been extensively tested in a realistic dynamic robotic simulator software: Gazebo, exploiting ROS as a programming framework, and the obtained results demonstrated the effectiveness of the navigation approach. Future directions of this work regard the possibility of adding obstacles in the repulsive field generation and deploying the proposed system on a real robotic platform to carry out tests in real-world environments.

Author Contributions: Conceptualization, J.C. and V.M.; Data curation, V.M.; Funding acquisition, F.R.; Investigation, J.C., V.M. and F.R.; Resources, J.C.; Supervision, F.R.; Writing—original draft, V.M. and J.C.; Writing—review and editing, J.C., V.M. and F.R. All authors have read and agreed to the published version of the manuscript.

Funding: The research leading to these results has been supported by the PRINBOT project, in the frame of the PRIN 2017 research program, grant number 20172HHNK5_002 and COWBOT project, in the frame of the PRIN 2020 research program, grant number 2020NH7EAZ_002.

Conflicts of Interest: The authors declare no conflict of interest.

References

1. Ferreira, J.; Moreira, A.P.; Silva, M.; Santos, F. A survey on localization, mapping, and trajectory planning for quadruped robots in vineyards. In Proceedings of the 2022 IEEE International Conference on Autonomous Robot Systems and Competitions (ICARSC), Feira, Portugal, 29–30 April 2022; pp. 237–242. <https://doi.org/10.1109/ICARSC55462.2022.9784796>.
2. Morlando, V.; Teimoorzadeh, A.; Ruggiero, F. Whole-body control with disturbance rejection through a momentum-based observer for quadruped robots. *Mech. Mach. Theory* **2021**, *164*, 104412. <https://doi.org/10.1016/j.mechmachtheory.2021.104412>.
3. Dudzik, T.; Chignoli, M.; Bledt, G.; Lim, B.; Miller, A.; Kim, D.; Kim, S. Robust Autonomous Navigation of a Small-Scale Quadruped Robot in Real-World Environments. In Proceedings of the 2020 IEEE/RSJ International Conference on Intelligent Robots and Systems (IROS), Las Vegas, NV, USA, 25–29 October 2020; pp. 3664–3671. <https://doi.org/10.1109/IROS45743.2020.9340701>.
4. Hu, X.; He, F.; Xiao, P.; Wang, T.; Zhang, D.; Zhou, X.; Fan, Y. Design of a Quadruped inspection Robot Used in Substation. In Proceedings of the 2021 IEEE 4th Advanced Information Management, Communicates, Electronic and Automation Control Conference (IMCEC), Chongqing, China, 18–20 June 2021; Volume 4, pp. 766–769. <https://doi.org/10.1109/IMCEC51613.2021.9482003>.
5. Chen, Z.; Fan, T.; Zhao, X.; Liang, J.; Shen, C.; Chen, H.; Manocha, D.; Pan, J.; Zhang, W. Autonomous Social Distancing in Urban Environments Using a Quadruped Robot. *IEEE Access* **2021**, *9*, 8392–8403. <https://doi.org/10.1109/ACCESS.2021.3049426>.
6. Morlando, V.; Selvaggio, M.; Ruggiero, F. Nonprehensile Object Transportation with a Legged Manipulator. In Proceedings of the 2022 International Conference on Robotics and Automation (ICRA), Philadelphia, PA, USA, 23–27 May 2022; pp. 6628–6634. <https://doi.org/10.1109/ICRA46639.2022.9811810>.
7. Bogue, R. Robots in the offshore oil and gas industries: A review of recent developments. *Ind. Robot. Int. J. Robot. Res. Appl.* **2020**, *47*, 1–6.
8. Hutter, M.; Sommer, H.; Gehring, C.; Hoepflinger, M.; Bloesch, M.; Siegwart, R. Quadrupedal locomotion using hierarchical operational space control. *Int. J. Robot. Res.* **2014**, *33*, 1047–1062. <https://doi.org/10.1177/0278364913519834>.
9. Xin, G.; Lin, H.C.; Smith, J.; Cebe, O.; Mistry, M. A Model-Based Hierarchical Controller for Legged Systems Subject to External Disturbances. In Proceedings of the 2018 IEEE International Conference on Robotics and Automation (ICRA), Brisbane, Australia, 21–25 May 2018; pp. 4375–4382. <https://doi.org/10.1109/ICRA.2018.8461172>.
10. Winkler, A.; Havoutis, I.; Bazeille, S.; Ortiz, J.; Focchi, M.; Dillmann, R.; Caldwell, D.; Semini, C. Path planning with force-based foothold adaptation and virtual model control for torque controlled quadruped robots. In Proceedings of the 2014 IEEE International Conference on Robotics and Automation (ICRA), Hong Kong, China, 31 May–7 June 2014; pp. 6476–6482. <https://doi.org/10.1109/ICRA.2014.6907815>.

11. Wermelinger, M.; Fankhauser, P.; Diethelm, R.; Krüsi, P.; Siegwart, R.; Hutter, M. Navigation planning for legged robots in challenging terrain. In Proceedings of the 2016 IEEE/RSJ International Conference on Intelligent Robots and Systems (IROS), Daejeon, Republic of Korea, 9–14 October 2016; pp. 1184–1189. <https://doi.org/10.1109/IROS.2016.7759199>.
12. Papadakis, P. Terrain traversability analysis methods for unmanned ground vehicles: A survey. *Eng. Appl. Artif. Intell.* **2013**, *26*, 1373–1385. <https://doi.org/10.1016/j.engappai.2013.01.006>.
13. Haddeler, G.; Chan, J.; You, Y.; Verma, S.; Adiwahono, A.H.; Meng Chew, C. Explore Bravelly: Wheeled-Legged Robots Traverse in Unknown Rough Environment. In Proceedings of the 2020 IEEE/RSJ International Conference on Intelligent Robots and Systems (IROS), Las Vegas, ND, USA, 25–29 October 2020; pp. 7521–7526. <https://doi.org/10.1109/IROS45743.2020.9341610>.
14. Ahtiainen, J.; Stoyanov, T.; Saarinen, J. Normal Distributions Transform Traversability Maps: LIDAR-Only Approach for Traversability Mapping in Outdoor Environments. *J. Field Robot.* **2017**, *34*, 600–621.
15. Haddeler, G.; Chuah, M.Y.M.; You, Y.; Chan, J.; Adiwahono, A.H.; Yau, W.Y.; Chew, C.M. Traversability analysis with vision and terrain probing for safe legged robot navigation. *Front. Robot. AI* **2022**, *9*, 887910–887910. <https://doi.org/10.3389/frobt.2022.887910>.
16. Khatib, O. Real-time obstacle avoidance for manipulators and mobile robots. In Proceedings of the 1985 IEEE International Conference on Robotics and Automation, St. Louis, MO, USA, 25–28 March 1985; Volume 2, pp. 500–505. <https://doi.org/10.1109/ROBOT.1985.1087247>.
17. Szczepanski, R.; Bereit, A.; Tarczewski, T. Efficient Local Path Planning Algorithm Using Artificial Potential Field Supported by Augmented Reality. *Energies* **2021**, *14*, 6642. <https://doi.org/10.3390/en14206642>.
18. Wu, E.; Sun, Y.; Huang, J.; Zhang, C.; Li, Z. Multi UAV Cluster Control Method Based on Virtual Core in Improved Artificial Potential Field. *IEEE Access* **2020**, *8*, 131647–131661. <https://doi.org/10.1109/ACCESS.2020.3009972>.
19. Huang, Y.; Ding, H.; Zhang, Y.; Wang, H.; Cao, D.; Xu, N.; Hu, C. A Motion Planning and Tracking Framework for Autonomous Vehicles Based on Artificial Potential Field Elaborated Resistance Network Approach. *IEEE Trans. Ind. Electron.* **2020**, *67*, 1376–1386. <https://doi.org/10.1109/TIE.2019.2898599>.
20. Harik, E.H.C.; Korsath, A. Combining Hector SLAM and Artificial Potential Field for Autonomous Navigation Inside a Greenhouse. *Robotics* **2018**, *7*, 22. <https://doi.org/10.3390/robotics7020022>.
21. Hongyu, H.; Chi, Z.; Yuhuan, S.; Bin, Z.; Fei, G. An Improved Artificial Potential Field Model Considering Vehicle Velocity for Autonomous Driving. *IFAC-PapersOnLine* **2018**, *51*, 863–867. <https://doi.org/10.1016/j.ifacol.2018.10.095>.
22. Cacace, J.; Finzi, A.; Lippiello, V. A mixed-initiative control system for an Aerial Service Vehicle supported by force feedback. In Proceedings of the 2014 IEEE/RSJ International Conference on Intelligent Robots and Systems, Chicago, IL, USA, 14–18 September 2014; pp. 1230–1235. <https://doi.org/10.1109/IROS.2014.6942714>.
23. Cacace, J.; Finzi, A.; Lippiello, V. Enhancing Shared Control via Contact Force Classification in Human-Robot Cooperative Task Execution. In *Human Friendly Robotics: 10th International Workshop*; Ficuciello, F., Ruggiero, F., Finzi, A., Eds.; Springer International Publishing: Cham, Switzerland, 2019; pp. 167–179.
24. Chilian, A.; Hirschmüller, H. Stereo camera based navigation of mobile robots on rough terrain. In Proceedings of the 2009 IEEE/RSJ International Conference on Intelligent Robots and Systems, St. Louis, MO, USA, 10–15 October 2009; pp. 4571–4576. <https://doi.org/10.1109/IROS.2009.5354535>.
25. Henze, B.; Ott, C.; Roa, M. Posture and balance control for humanoid robots in multi-contact scenarios based on model predictive control. In Proceedings of the 2014 IEEE/RSJ International Conference on Intelligent Robots and Systems, Chicago, IL, USA, 14–18 September 2014; pp. 3253–3258.
26. Ott, C.; Roa, M.A.; Hirzinger, G. Posture and balance control for biped robots based on contact force optimization. In Proceedings of the 2011 11th IEEE-RAS International Conference on Humanoid Robots, Bled, Slovenia, 26–28 October 2011; pp. 26–33.
27. Fahmi, S.; Mastalli, C.; Focchi, M.; Semini, C. Passive whole-body control for quadruped robots: Experimental validation over challenging terrain. *IEEE Robot. Autom. Lett.* **2019**, *4*, 2553–2560.
28. Henze, B.; Roa, M.A.; Ott, C. Passivity-based whole-body balancing for torque-controlled humanoid robots in multi-contact scenarios. *Int. J. Robot. Res.* **2016**, *35*, 1522–1543.
29. Caron, S.; Pham, Q.C.; Nakamura, Y. Stability of surface contacts for humanoid robots: Closed-form formulae of the contact wrench cone for rectangular support areas. In Proceedings of the 2015 IEEE International Conference on Robotics and Automation (ICRA), Seattle, WA, USA, 26–30 May 2015; pp. 5107–5112.
30. Murray, R.M.; Li, Z.; Sastry, S.S.; Sastry, S.S. *A Mathematical Introduction to Robotic Manipulation*; CRC Press: Boca Raton, FL, USA, 1994.
31. Selvaggio, M.; Cacace, J.; Pacchierotti, C.; Ruggiero, F.; Giordano, P.R. A shared-control teleoperation architecture for nonprehensile object transportation. *IEEE Trans. Robot.* **2021**, *38*, 569–583.
32. Morlando, V.; Ruggiero, F. Disturbance rejection for legged robots through a hybrid observer. In Proceedings of the 2022 30th Mediterranean Conference on Control and Automation (MED), Athens, Greece, 28 June–1 July 2022; pp. 743–748.
33. Marigold, D.S.; Patla, A.E. Strategies for dynamic stability during locomotion on a slippery surface: Effects of prior experience and knowledge. *J. Neurophysiol.* **2002**, *88*, 339–353.
34. Xu, P.; Ding, L.; Li, Z.; Yang, H.; Wang, Z.; Gao, H.; Zhou, R.; Su, Y.; Deng, Z.; Huang, Y. Learning physical characteristics like animals for legged robots. *Natl. Sci. Rev.* **2023**, *10*, nwad045.
35. Siciliano, B.; Sciavicco, L.; Villani, L.; Oriolo, G. Motion planning. *Robotics: Modelling, Planning and Control*; Springer: Berlin/Heidelberg, Germany, 2009; pp. 524–559.
36. Holt, C.C. Forecasting seasonals and trends by exponentially weighted moving averages. *Int. J. Forecast.* **2004**, *20*, 5–10.

37. Lucas, J.M.; Saccucci, M.S. Exponentially weighted moving average control schemes: Properties and enhancements. *Technometrics* **1990**, *32*, 1–12.
38. Caselli, S.; Reggiani, M.; Rocchi, R. Heuristic methods for randomized path planning in potential fields. In Proceedings of the 2001 IEEE International Symposium on Computational Intelligence in Robotics and Automation (Cat. No. 01EX515), Banff, AB, Canada, 29 July–1 August 2001; pp. 426–431.
39. Joseph, L.; Cacace, J. *Mastering ROS for Robotics Programming—Second Edition: Design, Build, and Simulate Complex Robots Using the Robot Operating System*, 2nd ed.; Packt Publishing: Birmingham, UK, 2018.

Disclaimer/Publisher’s Note: The statements, opinions and data contained in all publications are solely those of the individual author(s) and contributor(s) and not of MDPI and/or the editor(s). MDPI and/or the editor(s) disclaim responsibility for any injury to people or property resulting from any ideas, methods, instructions or products referred to in the content.